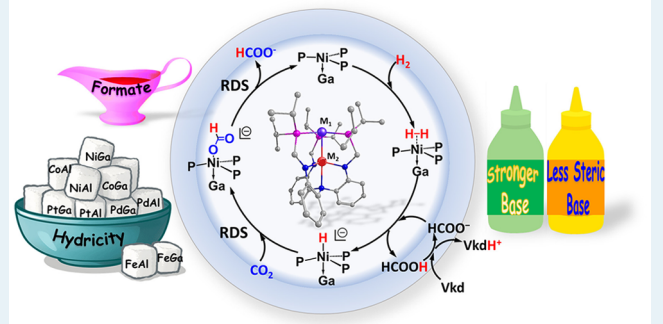
Rationalizing the Reactivity of Bimetallic Molecular Catalysts for CO₂ **Hydrogenation**

Jingyun Ye,*,†,‡® Ryan C. Cammarota,† Jing Xie,†,‡® Matthew V. Vollmer,† Donald G. Truhlar,†,‡® Christopher J. Cramer,†,‡® Connie C. Lu,*,†® and Laura Gagliardi†,‡®

Supporting Information

ABSTRACT: We have recently reported the heterobimetallic nickel-gallium complex, NiGaL (where L represents the tris(phosphinoamido)amine ligand, $[N(o-(NCH_2Pi-Pr_2))]$ $(C_6H_4)_3$ ³⁻), which is the most active Ni-based molecular catalyst for CO2 hydrogenation to date. Understanding the reaction mechanism of this catalytic system and identifying the factors that govern its catalytic activity are important in order to design even more efficient base-metal catalysts. Here, we present a computational study of possible reaction pathways for CO2 hydrogenation catalyzed by NiGaL. The most favorable predicted pathway for formate production agrees well with key experimental observations and is defined by four elementary steps: (1) H₂ binding to the Ni center, (2)



Recipes for Designing Bimetallic Molecular Catalysts for CO₂ Hydrogenation

deprotonation of the H2 adduct, (3) hydride transfer to CO2 to form a formate adduct, and (4) formate release to regenerate NiGaL. The overall catalytic process has two main time periods: an induction period, during which the deprotonation of the H₂ adduct by exogenous base is predicted to be rate-limiting, followed by a subsequent period where the produced formate assists in deprotonation by acting as a proton shuttle between the H₂ adduct and exogenous base. The barrier for H₂ adduct deprotonation is governed predominantly by the steric hindrance associated with the exogenous base and is found to be dramatically lowered by formate assistance. Once sufficient formate has been generated, the catalysis enters the steady-state period, during which hydride transfer to CO₂ is predicted to become rate-limiting once sufficient formate has been generated and the reaction rate remains constant until the base is nearly consumed. For hydride transfer to CO₂, the free energy of activation was found to depend linearly on the thermodynamic hydricity for a series of bimetallic $HM_1M_2L^-$ complexes, providing a simple and efficient strategy for screening other bimetallic catalysts. Furthermore, the relative binding energies of H₂ and formate were analyzed to predict the ability of the bimetallics to facilitate the catalytic turnover. The predicted trends and structure-activity relationships arising from these computational calculations can be further utilized for the rational design of more efficient catalysts for CO₂ hydrogenation and other hydride transfer processes for which reactive M-H species are generated in the presence of a Lewis base.

KEYWORDS: bimetallic complexes, H₂ deprotonation, CO₂ hydrogenation, basicity, steric hindrance, hydricity

1. INTRODUCTION

Fossil fuel combustion generates enormous quantities of carbon dioxide (CO₂) and has contributed significantly to the drastic rise of atmospheric CO₂ from a preindustrial level of 280 ppm to over 400 ppm in 2015. 1-4 The increase of atmospheric CO₂ is considered largely responsible for global warming through the greenhouse effect. 5,6 Catalytic hydrogenation of CO₂ has the potential to reduce net CO2 emissions while valorizing an abundant C1 source into renewable liquid fuels and valuable chemicals. $^{7-9}$ In the long term, this would be an efficient way to close the anthropogenic carbon cycle, provided that industrial CO_2 capture and sustainable H_2 production are also realized. $^{8,10-14}$ Hydrogenation of CO_2 to formic acid or formate is an attractive CO2 conversion reaction because

formic acid and formate salts are commercially valuable products and are promising liquid hydrogen carriers. 15-20 In past decades, great advances have been made to discover new, highly active catalysts for the production of formic acid and formate via CO₂ hydrogenation. ^{8,21,22} The most active catalysts are precious metal complexes of Ru, ^{23–29} Rh, ^{30–33} and Ir. ^{34–37} In 2009, Nozaki and co-workers obtained an excellent turnover number (TON) of 3,500,000 and turnover frequency (TOF) of 150,000 h⁻¹ for hydrogenation of CO₂ in aqueous KOH using an iridium-pincer trihydride complex, [Ir^{III}(H)₃(PNP)], where

Received: February 27, 2018 Revised: April 10, 2018 Published: April 13, 2018



[†]Department of Chemistry, University of Minnesota, Minneapolis, Minnesota 55455, United States

^{*}Minnesota Supercomputing Institute and Chemical Theory Center, University of Minnesota, Minneapolis, Minnesota 55455, United States

PNP is 2,6-bis((diisopropylphosphino)methyl)pyridine.³⁴ In 2014, Pidko and co-workers reported a pyridine-based Ru-PNP catalyst that gave an initial TOF of 1,892,000 h⁻¹ in the presence of DBU base at 132 °C.³⁸ However, the high cost and limited supply of precious metals (e.g., Ru, Rh, Ir) has provided a strong impetus to develop sustainable catalysts based on earth-abundant metals such as Fe, Co, and Ni.^{39–46} Recently, impressive catalytic performance has been achieved using Fe (TON \approx 58,990)⁴⁵ and Co (TON \approx 30,000)⁴⁶ pincer complexes. However, these catalysts require a Lewis acidic additive (e.g., LiBF₄,⁴⁵ LiOTf⁴⁶) to achieve their high activity, and in some cases the metal—pincer catalysts suffer from decomposition under the elevated temperatures utilized for catalysis.⁴⁶

We recently reported a bimetallic Ni–Ga catalyst, NiGaL⁴⁷ (Figure 1, where $M_1 = Ni$; $M_2 = Ga$; and L represents the

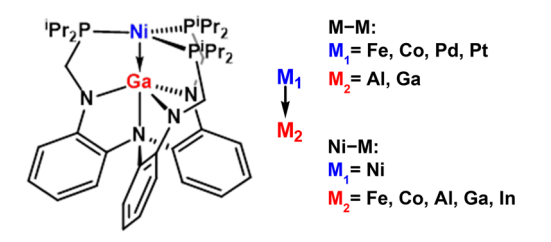


Figure 1. Structure of the NiGaL catalyst and other bimetallic pairings in this study.

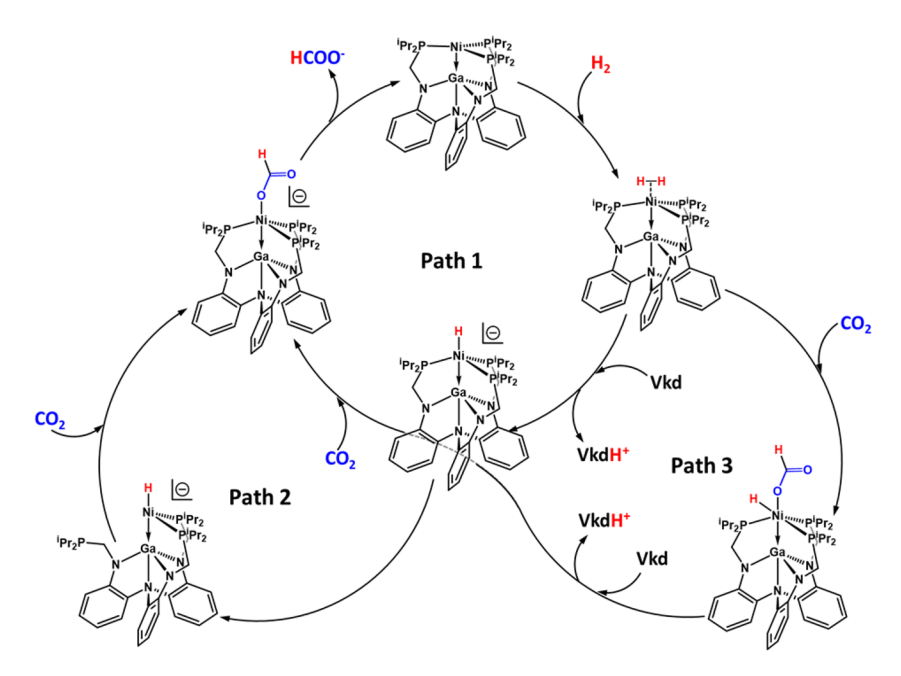
tris(phosphinoamido)amine ligand $[N(o-(NCH_2Pi-Pr_2)-C_6H_4)_3]^{3-})$. This complex features a Ni(0) \rightarrow Ga(III) dative bond, and it shows remarkable catalytic activity for hydrogenating CO₂ to formate as compared to prior homogeneous Ni-centered catalysts. ^{48–50} NiGaL catalyzed the reaction in tetrahydrofuran (THF) solvent at ambient temperature with a TON and an initial TOF of 3150 and 9700 h⁻¹, respectively, by utilizing Verkade's proazaphosphatrane, 2,8,9-triisopropyl-2,5,8,9-tetraaza-1-phosphabicyclo[3,3,3]undecane (abbreviated as Vkd iPr) as the stoichiometric base. Apart from being the

highest reported catalytic activity for a homogeneous Ni catalyst to date, this level of catalytic activity is generally impressive for a base metal catalyst operating at ambient temperature without any alkali metal additives. Near quantitative yields of formate were observed, with TON approaching the maximum value of 3200 under our catalytic conditions. Furthermore, in situ ³¹P NMR spectroscopy studies showed the formate adduct to be the predominant metal species after catalysis, indicating that TON was not limited by catalyst decomposition under optimal catalytic conditions. 47 In light of the stability and activity of the NiGaL catalyst, we sought to understand the catalytic reaction mechanism via the identification of important reaction intermediates and highbarrier reaction steps, with the goal of understanding the reaction mechanism so as to guide the design of more efficient base-metal catalysts. In this work, we present a computational study of possible reaction pathways for CO₂ hydrogenation catalyzed by NiGaL. In order to gain deeper insight into the reactivity-determining factors, the various intermediates and transition-state structures were studied in detail. Furthermore, we undertook a broader computational study of isostructural bimetallic complexes with varied bimetallic pairings (M_1-M_2) , which can be classified into two sets. In the first set, the Lewis acidic metal support (M_2) is either Al or Ga, and the catalytic active metal site (M₁) is Fe, Co, Pd, or Pt. In the second set, denoted as Ni-M2, the Lewis acidic site is Al, Ga, In, Fe, or Co, and the catalytic active metal site is Ni.

2. COMPUTATIONAL METHODS

Gaussian 09⁵¹ calculations were performed with the M06-L⁵² density functional using a def2-SVP basis set for C and H atoms that remain invariant during the reaction; a def2-TZVP basis set for N and P; and a def2-TZVPP basis set for Fe, Co, Pd, Pt Ni, Ga, Al, In, and the atoms involved in the reaction (C, O, and H atoms in CO₂, CO, HCO₂⁻, H⁻, H₂O, and H₂).^{53,54} The SDD effective core potential was used for Pd, In, and Pt.⁵⁵ The structures of all species were optimized in the gas phase. Harmonic vibrational frequencies were computed to confirm

Scheme 1. Three Possible Reaction Pathways for CO₂ Hydrogenation



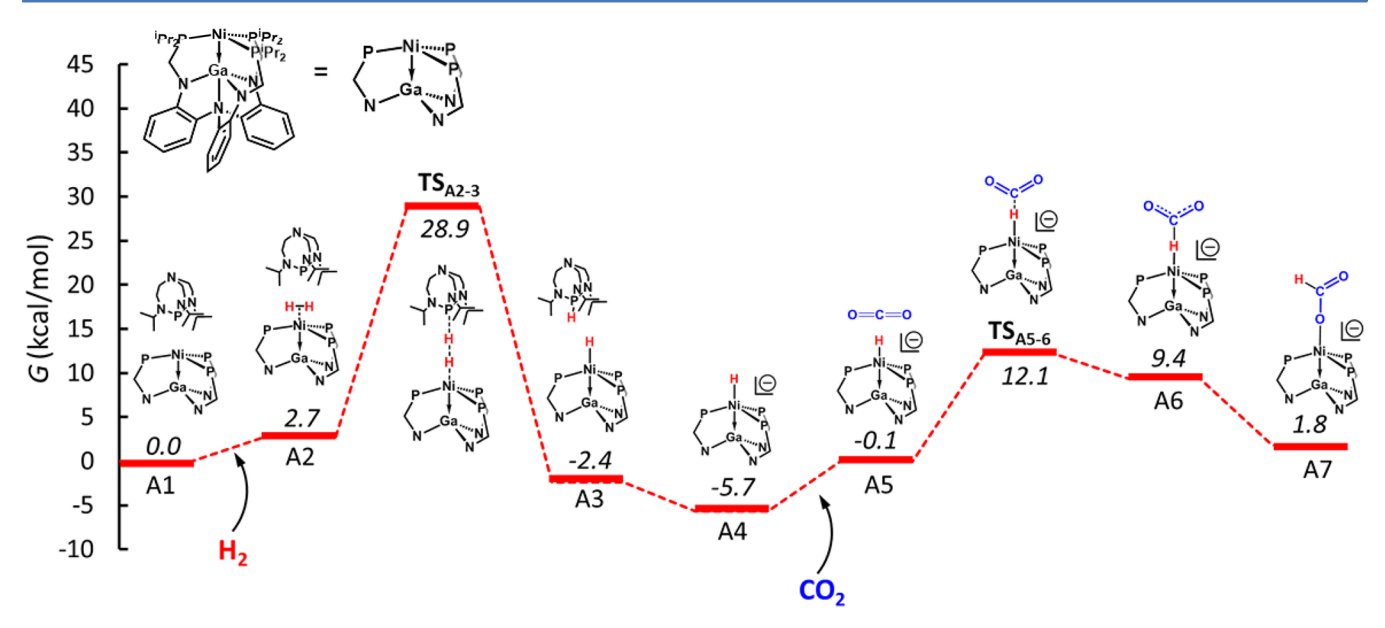


Figure 2. Gibbs free energy profile for CO₂ hydrogenation following path 1.

the nature of all intermediates (no imaginary frequencies) and transition state structures (one imaginary frequency). The gasphase Gibbs free energies, G, were calculated at T = 298.15 K and 1 atm pressure by using the harmonic approximation for the optimized structures. The solvation effect of tetrahydrofuran (THF) was included by performing single-point energy calculations at the gas-phase geometries using the SMD solvation model.⁵⁶ The relative solution-phase Gibbs free energies were calculated by adding solvation energies to the gas-phase relative Gibbs free energies. The Cartesian coordinates of all the structures and their associated electronic energies, enthalpies, and Gibbs free energies in both the gas phase and in solution are given in the Supporting Information. The energy values reported in the main text are Gibbs free energies (298.15 K, standard state of 1 atm for gases and 1 M for solutes) including the solvent effect of THF.

3. RESULTS AND DISCUSSION

3.1. The Reaction Mechanism for NiGaL-Catalyzed CO₂ Hydrogenation to Produce HCO₂⁻. The proposed reaction pathways for CO2 hydrogenation catalyzed by the NiGaL complex are shown in Scheme 1.47 Path 1 involves a sequence of four elementary steps: (1) H_2 binding to the d^{10} Ni(0) center to form an H₂ adduct, (η^2-H_2) NiGaL, (2) H₂ deprotonation, where (η^2-H_2) NiGaL is deprotonated by exogenous Verkade's base to form an anionic Ni hydride, [HNiGaL]-, which is ion-paired with protonated base [H-(Vkd iPr)]⁺, (3) hydride transfer to CO₂, where [HNiGaL]⁻ reacts with CO₂ via outer-sphere hydride transfer to generate the formate adduct, [(OCHO)NiGaL]-, and (4) formate release from [(OCHO)NiGaL] to give NiGaL, followed by the binding of H_2 to regenerate $(\eta^2 - H_2)$ NiGaL and restart the cycle. Path 2 shares the first two steps (H2 binding and deprotonation) and the last step (formate release) with path 1, but the intervening step involves the coordination of CO₂ to Ni prior to hydride migratory insertion, which necessitates the dissociation of one phosphine donor to open a coordination site at Ni for CO2. Thus, formation of the formate adduct in path 2 occurs via inner-sphere hydride transfer rather than direct, outer-sphere hydride transfer, as is invoked in path 1.

Alternatively, instead of deprotonation by an exogenous base after initial H_2 binding, path 3 involves direct hydride transfer from (η^2-H_2) NiGaL to CO_2 to produce (OCHO)(H)NiGaL, followed by deprotonation by Verkade's base to give $[(OCHO)NiGaL]^-$.

To verify that H₂ binding is the first step in the catalytic cycle, we compared the computed binding energies of H2 and CO_2 using the equation $\Delta G = G_{[L'NiGaL]} - G_{[NiGaL]} - G_{L'(g)}$, (L' = H₂ or CO₂). The Gibbs free energy for H₂ addition is calculated to be -0.4 kcal/mol, and the optimized structure of (η^2-H_2) NiGaL is provided in Figure S1a. For CO₂ addition, we found two possible binding modes, one in which CO₂ binds linearly to Ni, (η¹-CO2)NiGaL (Figure S1b), and another in which CO₂ binds to Ni in a bent fashion, $(\eta^2$ -CO₂)NiGaL (Figure S1c). Binding CO2 to Ni in either fashion was found to be endergonic by 15.6 and 21.2 kcal/mol for the linear and bent binding modes, respectively. These results suggest that CO₂ does not bind to NiGaL, and this allows us to rule out pathways in which formate is generated via initial CO2 activation. Our calculations predict that H₂ binding to NiGaL is thermodynamically favorable, which is consistent with the experiment in that H₂ binding to NiGaL was observed at 298 K and under 1 atm of H₂, whereas CO₂ binding was not observed at 298 K even under elevated pressures up to 34 atm of CO₂. 47 As a result, even though H₂ and CO₂ are introduced at the same time in catalytic reactions, the initial species formed is $(\eta^2$ H_2)NiGaL rather than a CO₂-bound species. Starting from (η^2 -H₂)NiGaL, we now discuss the detailed reaction energy profiles for the three pathways considered for NiGaL-catalyzed CO₂ hydrogenation.

Path 1. Under standard catalytic conditions, the initial concentration of Verkade's base (800 mM) is significantly higher than the concentration of the NiGaL catalyst (0.25 mM).⁴⁷ Hence, the initial structure in the reaction mixture is better described as the van der Waals complex [NiGaL]-[Vkd_iPr] (A1), rather than NiGaL. The binding of H₂ to A1 leads to the formation of a H₂ adduct [$(\eta^2$ -H₂)NiGaL]-[Vkd_iPr] (A2), which is endergonic by 2.7 kcal/mol. The Gibbs free energy profile for path 1 is shown in Figure 2, where

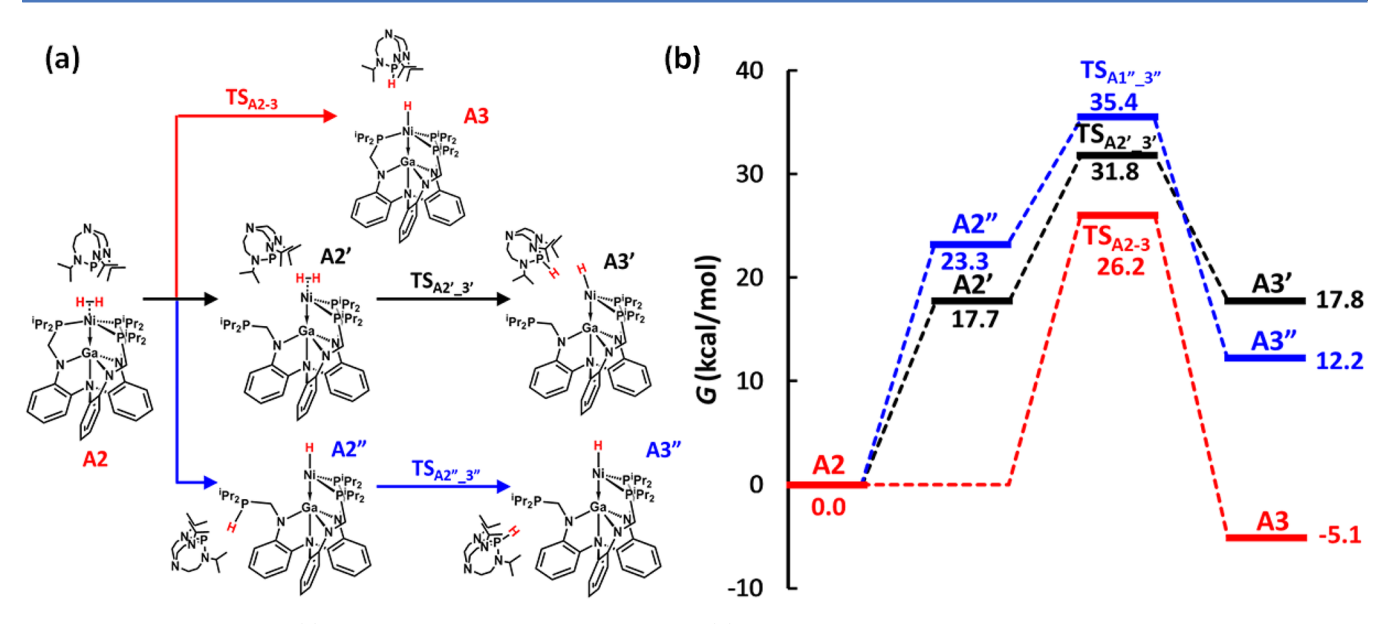


Figure 3. H₂ deprotonation: (a) three possible reaction mechanisms and (b) the Gibbs free energy profiles.

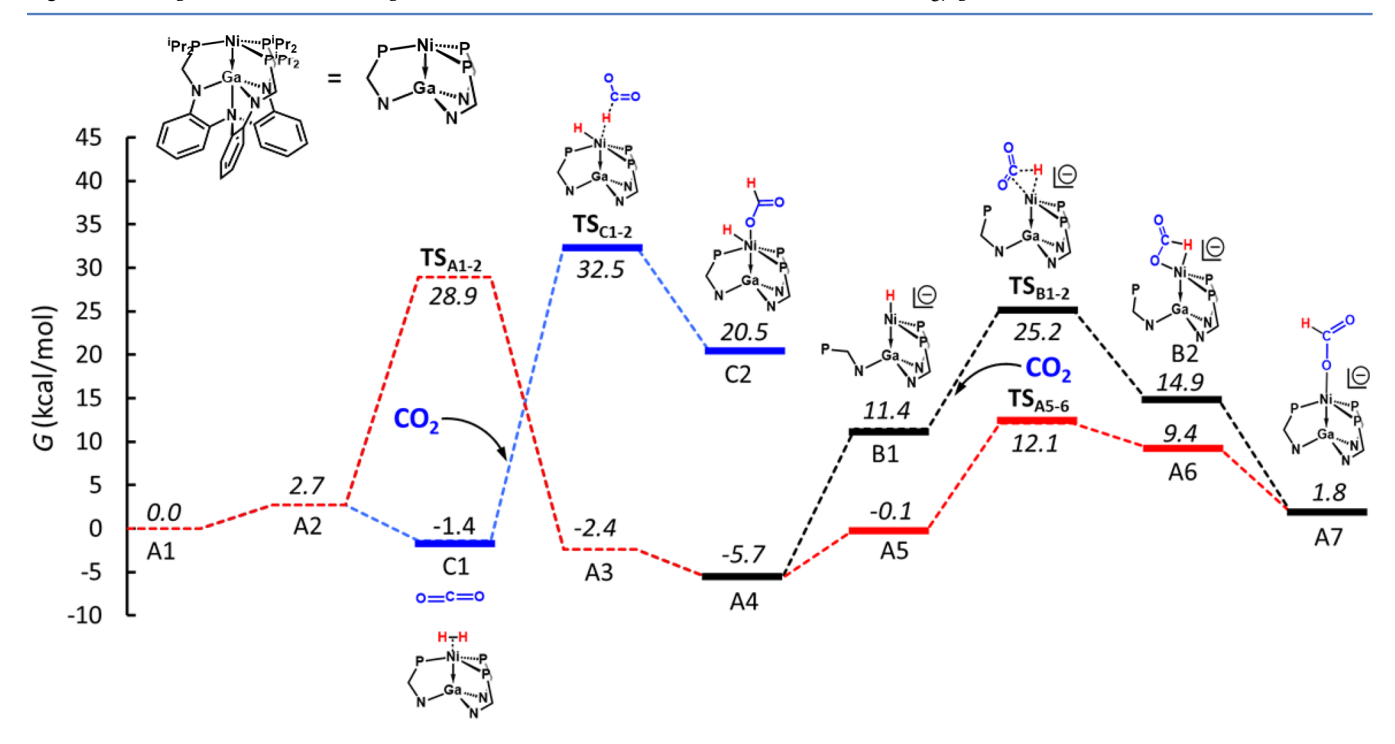


Figure 4. Gibbs free energy profile for CO_2 hydrogenation via alternative hydride transfer pathways, namely, through phosphine dissociation from the $[HNiGaL]^-$ adduct (A4, path 2, black line) and via CO_2 reacting directly with $(\eta^2-H_2)NiGaL$ (A2, path 3, blue line). Path 1 (red line) is also included as a reference.

the starting point is defined as separated [NiGaL][Vkd_iPr] (1 M in THF), H₂ (g, 1 atm), and CO₂ (g, 1 atm) at zero energy.

The H_2 adduct (A2) can be deprotonated by Verkade's base by three possible mechanisms as shown in Figure 3. The first mechanism (red path) involves Verkade's base approaching and deprotonating the H_2 adduct A2, which would occur via a transition structure TS_{A2-3} with a free energy of activation of 26.2 kcal/mol. The second mechanism (black path) involves the dissociation of one phosphorus donor, which provides more space for the Verkade's base to access and deprotonate the H_2 adduct. The overall Gibbs free energy of activation for H_2 deprotonation is 31.8 kcal/mol for this pathway (Figure 3b), which comprises the endergonic dissociation of one phospho-

rus donor to form A2' (17.7 kcal/mol) and the free energy of activation of 14.1 kcal/mol for the subsequent H_2 deprotonation from A2' via the transition state $TS_{A2'-3'}$. The third mechanism (blue path) involves one phosphine donor of the ligand serving as an internal base, followed by proton transfer from A2' to the external Verkade's base. As shown in Figure 3b, the third reaction mechanism has the largest free energy of activation (35.4 kcal/mol) of these three possible mechanisms for H_2 deprotonation. As a result, the first reaction mechanism involving the direct deprotonation of H_2 adduct by Verkade's base, without invoking any phosphine dissociation, is the most favorable mechanism for H_2 deprotonation. The Gibbs free energy of activation is 28.9 kcal/mol with respect to A1. The

product of H_2 deprotonation, the anionic Ni hydride complex that is ion-paired with protonated base, [H-(Vkd_iPr)]^+[HNiGaL]^- (A3), is more stable than A1 by 2.4 kcal/mol. The predicted thermodynamic favorability for H_2 deprotonation is validated by the experimental observation of quantitative conversion to $[H(Vkd_iPr)]^+[HNiGaL]^-$ upon the introduction of H_2 (1 atm) to a THF solution containing NiGaL and a slight excess (\geq 3 equiv) of Verkade's base. 47

The release of [H(Vkd iPr)]+ from the van der Waals complex, A3, stabilizes the Ni hydride [HNiGaL] (A4) by 2.7 kcal/mol. Subsequently, diffusion of CO2 to the Ni hydride generates the van der Waals complex, [HNiGaL]⁻[CO₂] (A5). Direct, outer-sphere hydride transfer to CO₂ through the transition structure TS_{A5-6} results in the formation of an Hbound formate adduct $[(\eta^1\text{-HCO}_2)\text{NiGaL}]^-$, A6. The Gibbs free energy of activation for outer-sphere hydride transfer to CO₂ is 12.2 kcal/mol with respect to the van der Waals complex A5, and 17.8 kcal/mol overall with respect to A4 and free CO₂. This latter barrier is very similar to the value of 17.2 kcal/mol computed for outer-sphere hydride transfer in THF from the similarly hydridic $HCo(dmpe)_2$ (where dmpe = dimethylphosphinoethane) to CO₂, which was predicted to be the rate-limiting step for the most active first-row metal catalytic system reported to date for CO₂ hydrogenation.⁵⁷ After hydride transfer, the H-bound formate adduct, A6, can release and rebind formate, or alternatively it can isomerize, to generate the O-bound formate adduct, $[(\eta^1\text{-OCHO})\text{NiGaL}]^-$ (A7), which is more stable than the H-bound isomer by 7.6 kcal/mol. Our calculations indicate that formate release and rebinding is favored over isomerization because the barrier for the isomerization of **A6** to **A7** is 5.2 kcal/mol, ⁵⁸ whereas formate release from the H-bound formate adduct is exergonic by 7.2 kcal/mol and predicted to be essentially barrierless, as shown in Figure S4a. Finally, the release of O-bound formate from A7 leads to the catalyst regeneration, which is slightly exergonic by 1.8 kcal/mol relative to A1 with no associated barrier (Figure S4b). In summary, the rate-determining step for path 1 is the direct deprotonation of the H₂ adduct by Verkade's base (Figure 2). The oxidation states of Ni and Ga do not change during the catalytic cycle.

Path 2. We investigated the likelihood of an inner-sphere hydride transfer to CO₂, which would contrast the outer-sphere reactivity studied in path 1. This is an important consideration because metal hydrides are well-known to undergo migratory insertion of the hydride ligand into bound, unsaturated substrates. ⁵⁹ Path 2, which is depicted in Figure 4 as a black line, begins with the same H2 binding and deprotonation steps as in path 1 to generate the anionic Ni hydride, A4. Path 2 then diverges to B1, where one phosphine donor has dissociated to generate an open coordination site at the Ni center that is adjacent to the hydride ligand. If CO₂ coordinates, then the resulting [(H)(CO₂)NiGaL]⁻ species would be ideally poised for hydride migratory insertion to CO₂. However, CO₂ binding to B1 to form [(H)(CO₂)NiGaL]⁻ (Figure S1d) with one unbound phosphine is energetically unfavorable by 13 kcal/ mol. Instead, after initial phosphine dissociation, B1 can react with CO₂ to generate an η^2 -O,H-formate adduct (B2) without prior coordination of CO₂ to Ni. The transition state TS_{B1-2} involves the hydride attacking CO2 and the phosphine donor moving toward and recoordinating to Ni in a concerted fashion. The distances between Ni and the P atom of the dissociated phosphine donor in TS_{B1-2} and B2 are 3.975 and 3.807 Å, respectively. Of note, these Ni···P distances are shorter than the

sum of their van der Waal radii (Ni, 2.14 Å; P, 2.1 Å),60 suggesting a somewhat stronger interaction than van der Waals forces between Ni and P. The Gibbs free energy of activation for CO₂ directly reacting with the hydride of B1 to produce the formate adduct B2 is 13.8 kcal/mol. Since the dissociation of the phosphorus donor requires 17.1 kcal/mol of free energy, the overall Gibbs free energy of activation for hydride transfer via this pathway is 30.9 kcal/mol, which is higher than the free energy of activation for H₂ deprotonation (28.9 kcal/mol). B2 converts to A7 through isomerization of the coordinated formate and recoordination of the dissociated phosphine donor to Ni, which collectively is exergonic by 13.1 kcal/mol. Thus, the rate-determining step for path 2 is hydride transfer at a diphosphine Ni site. By comparison, outer-sphere hydride transfer (path 1) from a triphosphine-coordinated Ni hydride only has a free energy of activation of 12.2 kcal/mol, which is ~18 kcal/mol more favorable than that for path 2, with the difference almost entirely attributable to the unfavorable dissociation of a phosphorus donor to accommodate the incoming CO₂ ligand.

Path 3. Rather than hydride transfer occurring after initial deprotonation of H2, CO2 could alternatively react directly with the dihydrogen adduct according to the potential energy profile shown in Figure 4 (depicted as a blue line). After the H₂ adduct (A2) forms, the diffusion of CO2 results in a van der Waals complex $[(\eta^1-H_2)NiGaL][CO_2]$, C1, which is -1.4 kcal/mol lower in energy than A1. The Gibbs free energy of activation for direct hydride transfer from the H₂ adduct to CO₂ was found to be 33.9 kcal/mol, which is higher than that for the rate-determining steps in both path 1 and path 2. From C2, path 3 would be completed by HCO2- release and deprotonation of the Ni-H by Vkd_iPr, which can occur in either order or in a concerted fashion. We did not further investigate path 3 because the free energy of activation for hydride transfer from the H₂ adduct to CO₂ is too high to compete with the other pathways. On the basis of the experimental observations, we also ruled out a similar pathway involving initial H₂ oxidative addition to give a Ni(II) dihydride species, followed by reaction with CO2 to give C2. We previously observed that no isotopic scrambling of a mixture of H₂/D₂ to HD was observed for NiGaL, which would be expected to be facile if a Ni(II) dihydride species was energetically accessible.⁶¹ Additionally, only the H₂ adduct was observed upon the addition of a mixture of H2/CO2 to NiGaL in the absence of base, indicating that neither the H₂ adduct nor any Ni(II) dihydride species that could potentially be formed was hydridic enough to react with CO₂ to generate C2.47,61

In summary, path 1 is the lowest-energy pathway, with the key steps being the deprotonation of the H_2 adduct with Verkade's base and outer-sphere hydride transfer from the resulting anionic Ni–H species to CO_2 . We have ruled out alternative hydride transfer pathways, including hydride migratory insertion to a bound CO_2 with the dissociation of a phosphine donor, and the direct reaction between the H_2 adduct and CO_2 , which would side-step the formation of a discrete anionic Ni hydride, [HNiGaL]⁻. Indeed, [HNiGaL]⁻ has been isolated, and its estimated thermodynamic hydricity value of ~ 31 kcal/mol in CH_3CN (see section 3) provides a significant driving force for outer-sphere hydride transfer to CO_2 . Instead of hydride transfer, the rate-determining step for path 1 is the deprotonation of the H_2 adduct by Vkd_iPr. The calculated free energy of activation of 26.2 kcal/mol is larger

than expected for a catalytic process occurring readily at room temperature. 47 Hence, we were inspired to investigate in greater detail the factors that affect the activation energy for H_2 deprotonation.

3.2. The Importance of Basicity and Steric Effects of the Base in H_2 Deprotonation. In light of the finding that the rate-determining step for path 1 is the H_2 deprotonation, it follows that catalytic activity could potentially be improved by modifying the factors that govern the energetics of this step. First, the base used in CO_2 hydrogenation plays an important role, as discussed in previous experimental studies. ^{47,62,63} As shown in Figure 5, we have investigated four bases with varying

Figure 5. Two Verkade's super bases (Vkd_Me and Vkd_iPr) and two guanidine bases (TMG and tBuTMG) and the pK_a values of their conjugate acids in CH₃CN.

basicity and steric hindrance in order to gauge how these two factors influence the favorability of H2 deprotonation. Specifically, this study includes two Verkade's super bases, 2,8,9-trimethyl-2,5,8,9-tetraaza-1-phosphabicyclo[3,3,3] undecane (abbreviated as Vkd Me) and Vkd iPr, and two guanidine bases, 1,1,3,3-tetramethylguanidine (abbreviated as TMG) and 2-(tert-butyl)-1,1,3,3-tetramethylguanidine (abbreviated as tBuTMG). Their base strengths are assessed by the reported p K_a values of the conjugate acids, where a higher p K_a value corresponds to a stronger base. The pK_a values for the conjugate acids of Vkd_Me, Vkd_iPr, TMG, and tBuTMG are 32.9, 64 33.6, 64 23.4, 65 and 26.5, 62,63 respectively, in CH₃CN. In addition, the formate product, HCO₂-, can serve as a proton acceptor once it is generated in the catalytic reaction. The pK_a value for HCO₂⁻ in THF is experimentally unavailable, but the computationally estimated pK_a value for CH₃COOH in THF is 22.1,66 which should be comparable to the pK_a value of HCOOH. As a result, we also studied the potential role of HCO₂⁻ in the H₂ deprotonation step. The potential energy profiles for H₂ deprotonation by these bases are shown in Figure 6. In analogy to path 1, the geometries of reactant (A2*), transition state (TS_{A2-3}*), and product (A3*) are similar to those calculated for Verkade's base (Vkd iPr) in section 1.

Basicity. Of the bases shown in Figure 5 for which the deprotonation of the H₂ adduct was computed, only Vkd_iPr and tBuTMG were employed experimentally in catalysis. Comparing these two bases, the Gibbs free energy of activation for H₂ deprotonation is slightly greater for tBuTMG (27.8 kcal/mol) than for the more basic Vkd_iPr (26.2 kcal/mol). While the steric effect of the base was not probed explicitly experimentally, decreasing the basicity of the base was seen to result in more sluggish catalystic rates and/or no catalytic

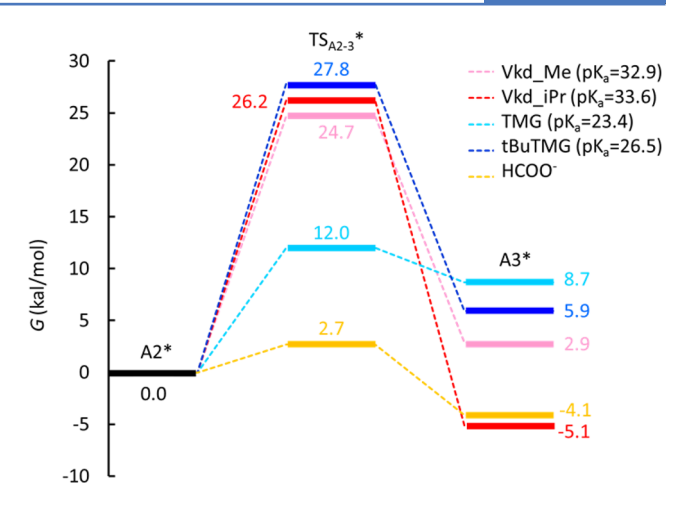


Figure 6. Effect of basicity and steric hindrance of bases on the H_2 deprotonation step. $A2^*$ and $A3^*$ represent the van der Waals complexes $[H_2NiGaL][base]$ and $[Hbase]^+[HNiGaL]^-$, respectively. TS_{A2-3}^* represents the transition state from $A2^*$ to $A3^*$.

formate generation. Specifically, the overall turnover frequency (TOF) using tBuTMG is 80 h-1, which is significantly lower than the overall TOF of 2130 h⁻¹ using Vkd_iPr under identical catalytic conditions and qualitatively consistent with the respective barriers to H_2 deprotonation for the two bases.⁴⁷ The use of an even weaker base, NEt₃ (p $K_a = 18.8$), was also investigated experimentally, and no formate was detected.⁴⁷ In the case of Vkd Me, the free energy of activation for H₂ deprotonation is 24.7 kcal/mol, which is lower than that for Vkd iPr by 1.5 kcal/mol. This finding was initially surprising because Vkd Me is a weaker base than Vkd iPr. The results for TMG are even more dramatic: the corresponding free energy of activation for H₂ deprotonation is 12.0 kcal/mol, which is by far the lowest among the bases in Figure 5, even though TMG is the weakest of the four bases. These intriguing results inspired us to study in detail the structures of the initial state (A2*), transition state (TS_{A2-3}^*) , and final state $(A3^*)$ for H_2 deprotonation to identify the role that steric hindrance plays in this particular reaction, as the low barrier for deprotonation with TMG could potentially be attributable to the fact that it is the least sterically hindered among the bases studied (Figure 5).

Steric Effects. To understand the steric effect of the base on the H₂ deprotonation step, the structures of the initial state (A2*), transition state (TS_{A2-3}*), and final state (A3*) were calculated and analyzed for the bases shown in Figure 5, and the structural details are summarized in Tables S1-S4. We identified a single geometric parameter that is highly sensitive to the steric hindrance of the base, namely, the distance between Ni and the P atom (for Verkade's bases) or the N atom (for guanidine bases), which is denoted as $d(Ni\cdots P/N)$. This parameter seems sensible because H₂ deprotonation requires the close approach of base in the van der Waals complex, $[(\eta^2-H_2)NiGaL][base]$, to allow for direct proton transfer from (η^2-H_2) NiGaL to the base. As shown in Figure 7b, $d(Ni\cdots P/N)$ in A2*, TS_{A2-3} *, and A3* is significantly longer for the bulkier bases such as Vkd iPr and tBuTMG, compared to their less bulky counterparts, Vkd Me and TMG, respectively. The larger values of $d(Ni\cdots P/N)$ in the precursor complexes A2* seem to track with the greater activation barriers for H₂ deprotonation. Specifically, the Gibbs free energy of activations for tBuTMG (27.8 kcal/mol) and Vkd iPr (26.2 kcal/mol) are larger compared to those of

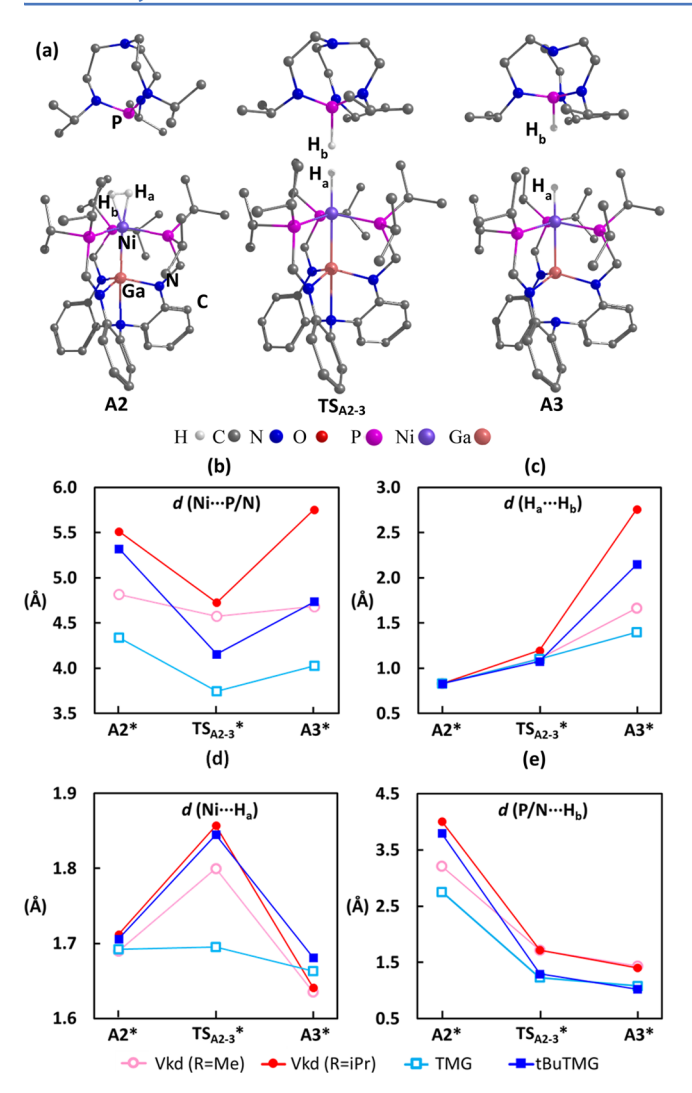


Figure 7. (a) The structures of $A2^*$, TS_{1-2}^* , and $A3^*$ shown for Vkd_iPr base. Except for the H_2 or H_2 -derived protons, all other protons are omitted for clarity. The variation of distance between (b) Ni and P/N of base, $d(Ni\cdots P/N)$, (c) H_a and H_b , $d(H_a\cdots H_b)$, (d) Ni and H_a and H_b , $d(Ni\cdots H_a)$, and (e) P/N of the base and H_b , $d(P/N\cdots H_b)$, are shown for $A2^*$, TS_{1-2}^* , and $A3^*$ along the pathway of H_2 deprotonation.

their less bulky TMG (12.0 kcal/mol) and Vkd_Me (24.7 kcal/mol) analogs, respectively. This analysis shows that the order of the free energies of activation for the deprotonation reaction at the relatively hindered Ni site are largely dictated by steric effects, such that a base with weaker basicity and less steric bulk (e.g., TMG) can have lower free energies of activation for $\rm H_2$ deprotonation than bases with stronger basicity and greater steric hindrance (e.g., Vkd_Me, Vkd_iPr, tBuTMG).

In Figure 7c–e, the $d(H_a \cdots H_b)$, $d(\text{Ni} \cdots H_a)$, and $d(\text{P/N} \cdots H_b)$ distances are plotted along the reaction coordinate for H_2 deprotonation. By examining these plots, we identified three distances that are sensitive to the steric hindrance of the base: $d(\text{P/N} \cdots H_b)$ in $A2^*$, $d(\text{Ni} \cdots H_a)$ in TS_{A2-3}^* , and $d(H_a \cdots H_b)$ in $A3^*$. Of interest, the $H_a \cdots H_b$ distance in $A2^*$ and the $Ni \cdots H_a$ distance in $A2^*$ and $A3^*$ are essentially invariant with all bases (see Figure 7c,d and Table S2), presumably because they depend more on the electronic properties of the Ni center and its interaction with either the H_2 or the hydride ligands, and thus are not directly impacted by the base. In addition, d(P/

 $N \cdots H_b$) of TS_{A2-3}^* and $A3^*$ is not sensitive to the sterics or basicity of the base but rather depends simply on whether the proton acceptor is a P or N atom. Due to the near linearity of the $d(Ni\cdots H_a)$, $d(H_a\cdots H_b)$, and $d(P/N\cdots H_b)$ vectors in the transition state TS_{A2-3}^* , the Ni···P/N distance in TS_{A2-3}^* can be approximated by the equation $d(Ni\cdots P/N) \approx d(Ni\cdots H_a) +$ $d(H_a \cdots H_b) + d(P/N \cdots H_b)$. As shown in Figure 7b-e, the $d(H_a \cdots H_b)$ and $d(P/N \cdots H_b)$ do not vary much in TS_{A2-3}^* ; however, d(Ni···H_a) does show a large variation for the different bases. For example, the $d(Ni\cdots H_a)$ of TS_{A2-3}^* for TMG is much shorter than that for the other bases, and thus it is much closer to the optimal d(Ni···H_a) in the resulting hydride that forms, A3*. In other words, the low steric hindrance of TMG allows for closer approach of the "base(P/ N)... H_h ... H_a " unit to Ni, which allows for a shorter $d(Ni...H_a)$ that will require less rearrangement to achieve the optimal d(Ni···H_a) in A3*. This results in the Gibbs free energy of activation for deprotonation by TMG being much lower than for the other three bases, which counters the aforementioned trend in basicity strengths. Although the basicity is not as important as steric effects in determining the barrier to H₂ deprotonation, the use of a strong base is still crucial for catalysis because the proton transfer from (η^2-H_2) NiGaL (pK_2) \approx 33.1 in CH₃CN) to the base is only an exergonic process for Vkd iPr $(pK_3 = 33.6)$ and is endergonic for Vkd Me, tBuTMG, and TMG. Nonetheless, the relative free energies of activation for the deprotonation of (η^2-H_2) NiGaL with various bases highlight the significant influence that steric considerations can have, as the bulky isopropyl groups on the phosphines of the ligand hinder a close approach of the exogenous base. Hence, the steric hindrance of the exogenous base and the ligand phosphine substituents are both important experimental parameters to vary for further optimization of the current catalytic system. 67,68

Formate As a Base. As shown in Figure 6, the free energy of activation for H₂ deprotonation using formate as a proton acceptor is only 2.7 kcal/mol, which is significantly lower than the barriers for Verkade's super bases and for the TMG and tBuTMG guanidine bases. This is consistent with Urakawa's calculations that it is barrierless for H transfer to formate on $[Ru(H)_2]$ complex, which is more active than $(\eta^2-H_2)NiGaL$ because a dihydride complex forms on Ru(dmpe)2, while for the $(\eta^2$ -H₂)NiGaL complex, H₂ is in molecular form.^{58,69} This dramatically lower free energy of activation indicates that it is favorable for formate to assist in H₂ deprotonation by acting as a proton shuttle: the less bulky formate can approach $(\eta^2$ H₂)NiGaL more readily than can a stronger but bulkier base. When the Vkd iPr base is present in solution, formate can readily transfer the proton it accepted from (η^2-H_2) NiGaL to Vkd iPr, and this transfer is exergonic by 4.2 kcal/mol. After the downhill transfer of the proton to Verkade's base, formate is regenerated and can further participate as a base in subsequent H₂ deprotonation events, as shown in Figure 8. This prediction is consistent with experimental observations that the catalysis stops when Vkd iPr has been consumed, as a sufficiently strong base is needed to drive the overall catalytic reaction starting from H₂ and CO₂, which is a favorable reaction when generating formate in organic solvent but not favorable when producing formic acid. 70-72,13,12 Of note, the reverse reaction where the Ni hydride is reprotonated by formic acid is relatively facile with a low free energy of activation of 6.8 kcal/mol; however, this is outcompeted by the exergonic proton transfer

Figure 8. H_2 deprotonation by Verkade's base assisted by formate, along with the relevant structures where formate acts as a proton shuttle (A2*, TS₂₋₃*, and A3*). Note that the values labeled in the structures are selected bond distances in Å.

from HCOOH to Vkd_iPr to produce formate when sufficient base is present in the reaction mixture.

We conclude that the CO₂ hydrogenation reaction catalyzed by NiGaL is initiated with Vkd_iPr as the direct protonacceptor until enough formate is generated in solution to serve as a proton shuttle between the H₂ adduct and Vkd_iPr. Therefore, as formate builds up with time, the reaction rate

should increase until sufficient formate exists in the solution, at which point the rate will be constant (i.e., linear HCOO vs time kinetics plot) until it is slowed by the depletion of base. With the strongly basic Vkd iPr, the formate product is generated very quickly (initial TOF = 9700 h^{-1}), and so this postulated rate increase during the initial buildup of formate was not observed.⁴⁷ However, upon substituting Vkd_iPr base with tBuTMG under otherwise identical conditions, the CO₂ hydrogenation reaction was found to have two distinct time periods: (1) an induction period for the first ~ 3 h, during which the reaction rate accelerates slowly until about ~100 equiv HCO_2^- are generated relative to catalyst, and then (2) a period from ~3.5 to 7.5 h, during which time the reaction rate remains constant at 120 h⁻¹ (the maximum rate reached at the end of the induction period) until tBuTMG is nearly consumed.⁴⁷ Thus, the two kinetic periods observed for tBuTMG lend support to the computationally proposed mechanism for H₂ deprotonation. The low basicity and high degree of steric hindrance for tBuTMG likely hinder the deprotonation step. Once sufficient formate has been generated, the reaction rate accelerates as formate acts as a cocatalyst in the H₂ deprotonation step.

The proposal that formate can act as an intermediary base to generate formic acid, which then undergoes proton transfer to the stoichiometric Vkd_iPr base, is consistent with the observation of very low concentrations of formic acid during catalysis only when nearly all the Vkd_iPr base has been consumed (1 equiv formic acid relative to 5 equiv of formate for trials with 0.25 mM NiGaL catalyst under 34 atm H₂/CO₂, Figure S2). We interpret this observation as suggestive that proton transfer between formate and Vkd_iPr becomes slow on the NMR time scale, and thus observable, only when Vkd_iPr has been depleted and is not readily present in high concentration to readily accept the proton. As a counterargument, the formation of formic acid could also result from the

Scheme 2. Most Favorable Pathway for CO₂ Hydrogenation

weak base equilibrium of [H(Vkd iPr)]+[HCO₂] as the concentration of the free Vkd iPr base approaches zero. However, the exceedingly large difference of ~ 11 pK_a units between [H(Vkd_iPr)]+ and formic acid (vide supra) would imply that any formic acid generated from the weak base equilibrium of [H(Vkd iPr)]+[HCO₂] would likely be too minute to be observed by standard ¹H NMR spectroscopy. Overall, the remarkably low free energy of activation for H₂ deprotonation by formate relative to Vkd iPr and the other bases examined means that with sufficient buildup of formate, the rate-determining step for path 1 will switch from H₂ deprotonation to outer-sphere hydride transfer to CO2 during the time course of the catalysis. In summary, the most favorable reaction path (Scheme 2) starts with H2 binding, followed by H₂ deprotonation where formate acts as a proton shuttle which transfers a proton from the H2 adduct to Verkade's base, resulting in the anionic Ni hydride species [HNiGaL] and the protonated base [H(Vkd iPr)]+. Formate produced through the outer-sphere hydride transfers to CO₂. Finally, the catalytic cycle is completed by release of formate.

3.3. Effect of Hydricity on CO_2 Hydrogenation. Thermodynamic hydricity $(\Delta G^{\circ}_{H^{-}})$ is an important quantitative parameter, which can be applied to evaluate the propensity of a metal hydride, M–H, to transfer a hydride to a substrate. It is defined as the free energy change for the reaction: $MH^n \rightarrow M^{n+1} + H^{-70,73,74}$ and in the present work we use

$$\Delta G^{\circ}_{H^{-}} = G([M_{1}M_{2}L] + G(H^{-}) - G([HM_{1}M_{2}L]^{-})$$
 (1)

The $\Delta G^{\circ}_{H^{-}}$ values for stable metal hydrides are always positive because it requires energy input to cleave a M-H bond to generate a discrete hydride (i.e., H⁻), and the hydricity of eq 1 is positive for a stable metal hydride. A larger ΔG°_{H} value for a metal hydride indicates that the release of a hydride is more thermodynamically unfavorable, whereas a lower $\Delta G^{\circ}_{H^{-}}$ indicates a stronger hydride donor. The thermodynamic hydricity of the resulting metal hydride generated from H₂ deprotonation is a key consideration for hydride transfer to CO₂ and for the overall activity of CO₂ hydrogenation, especially in light of the dramatic lowering of the deprotonation barrier by formate assistance which results in the prediction that hydride transfer becomes rate-limiting. 70 To determine the relationship between the thermodynamic hydricity (ΔG°_{H}) of a metal hydride and the free energy of activation (ΔG^{\ddagger}) for hydride transfer to CO₂, a variety of bimetallic complexes were studied, as shown in Figure 1. We have previously found that bimetallic complexes pairing first-row metals (Fe, Co, Ni) with group 13 supporting metals (M = Al, Ga, and In) are best described as Fe(0), Co(0), and Ni(0) with a M(III) supporting ion. 47,61,75 Thus, a singlet spin state is preferred for Ni(0) bimetallics, and the highest possible spin state is preferred when the supporting metal is Fe or Co (Table S5). In our previous work, the ground states of Fe-Al and Co-Al were identified to be a triplet and doublet, respectively, which correspond to Fe(0)-Al(III) and Co(0)-Al(III) metal pairings.⁷⁵ This agrees with the established principle that the +3 oxidation state is the most stable oxidation state for Al and Ga ions, as the inert pair effect does not come into play until heavier group 13 elements like Tl are considered. As a result, all complexes were considered to be zero-valent transition metals supported by a trivalent supporting group 13 metal. A linear relationship between ΔG^{\ddagger} for hydride transfer to CO_2 and $\Delta G^{\circ}_{H^-}$ of the metal hydride is identified for M-M and Ni-M complexes, with a coefficient of determination (R^2) of 0.88 and 0.90,

respectively, as shown in Figure 9. The linear relationship can be rationalized by noting that a stronger hydride donor (low

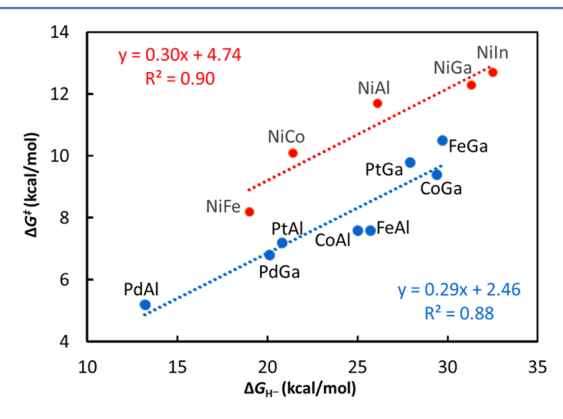


Figure 9. Calculated Gibbs free energy of activation for the outersphere hydride transfer to CO_2 (ΔG^{\ddagger}) on $[\mathrm{HM}_1\mathrm{M}_2\mathrm{L}]^-$ as a function of the calculated hydricity of metal—metal ($\mathrm{M}_1\mathrm{M}_2$) hydride in THF ($\Delta G^\circ_{\mathrm{H}^-}$). ΔG is calculated using the equation $\Delta G^{\ddagger} = G(\mathrm{TS}_{\mathrm{AS-6}}) - G([\mathrm{CO}_2][\mathrm{HM}_1\mathrm{M}_2\mathrm{L}]^-)$. Hydricity values were calculated using eq 1 and then referenced to the experimentally determined ΔG_{H^-} value of 31.3 kcal/mol⁴⁷ for [HNiGaL]⁻ in CH₃CN.

 $\Delta G^{\circ}_{H^{-}})$ readily transfers to CO_{2} (low ΔG^{\ddagger} for hydride transfer), whereas a weaker hydride donor requires more activation energy to react with CO_{2} . The correlation shown in Figure 9 indicates that the activation barriers for hydride transfer to CO_{2} for the bimetallic complexes studied can be estimated fairly accurately from the thermodynamic hydricity, which can, in principle, be measured from the experiment. Furthermore, this relationship gives us a useful catalyst descriptor for screening other bimetallic complexes rather than computing the free energies of activation for an entire mechanistic pathway to identify potential catalysts. The slopes of the two linear relations in Figure 9 are similar, with the red line (Ni–M) lying about 2 kcal/mol higher than the blue line (M–Al and M–Ga).

All of the anionic bimetallic hydrides shown in Figure 9 are hydridic enough for spontaneous hydride transfer to CO_2 (i.e., $\Delta G^{\circ}_{H^-}$ ([HM₁M₂L]⁻) < $\Delta G^{\circ}_{H^-}$ (HCO₂⁻) = 44 kcal/mol in CH₃CN). However, it is important to note that while a low barrier to hydride transfer is seemingly beneficial to catalysis, there is an inherent trade-off regarding the stability and reactivity of a metal hydride. An unstable metal hydride, characterized by a low $\Delta G^{\circ}_{H^-}$, will likely facilitate rapid and favorable hydride transfer, but its formation via deprotonation of a metal—dihydrogen adduct would also become more difficult. ^{74,78} With these considerations in mind, the best bimetallic catalysts among this set are likely the systems where the corresponding bimetallic hydrides have $\Delta G^{\circ}_{H^-}$ values between 30 and 44 kcal/mol, e.g., Fe—Ga, Co—Ga, Ni—Ga, and Ni—In.

3.4. Comparing Binding Energies of H_2 , HCO_2^- , and CO. In addition to the consideration of H_2 deprotonation and hydride transfer to CO_2 , the binding of H_2 , HCO_2^- , or CO to these bimetallic complexes can also play an important role in CO_2 hydrogenation. Highly active catalysts for CO_2 hydrogenation should have relative binding energies that allow the release of formate (HCO_2^-) and subsequent binding of H_2 , as catalytic turnover will be impeded, stopped, and/or require high H_2 pressure if formate binds too strongly. 58,69 In addition, we consider CO binding because CO has been reported as a

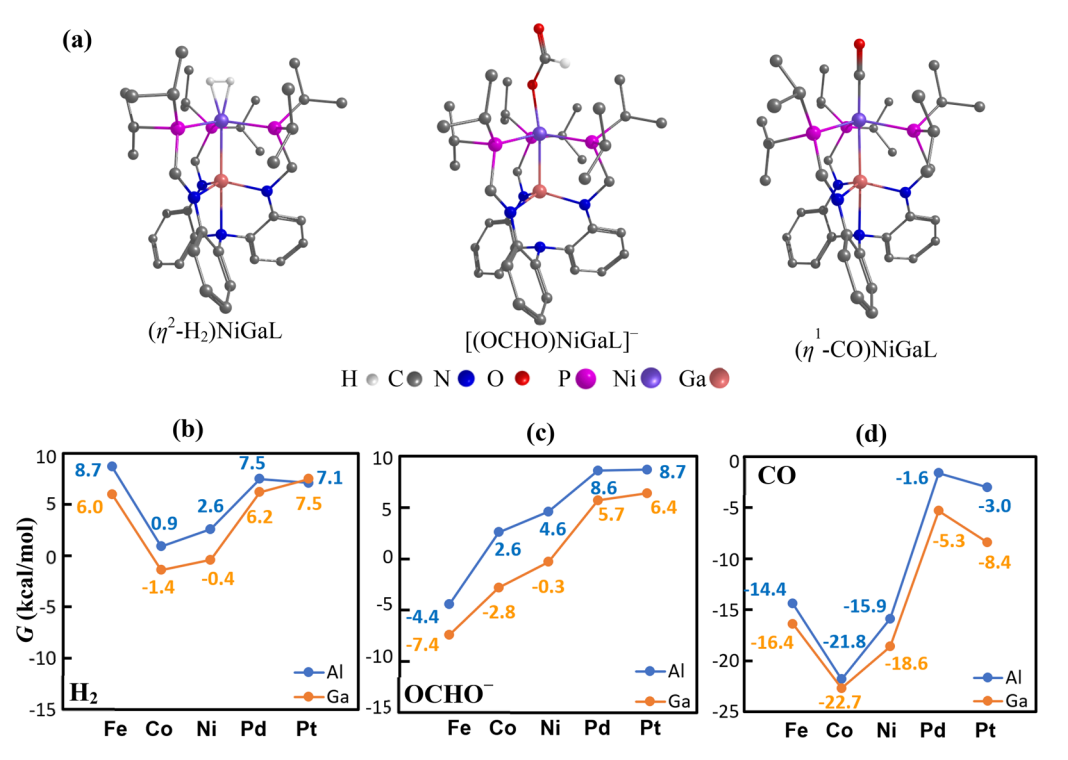


Figure 10. (a) The structures of $(\eta^2\text{-H}_2)\text{NiGaL}$, $[(\text{OCHO})\text{NiGaL}]^-$, and $(\eta^1\text{-CO})\text{NiGaL}$ (H atoms bound to carbons are not shown for clarity). The binding free energies of H₂, OCHO⁻, and CO on M₁M₂L (M₁ = Fe, Co, Ni, Pd, Pt; M₂ = Al, Ga) are plotted in b, c, and d.

byproduct of CO_2 hydrogenation catalysis via either the reverse water—gas shift reaction or formate dehydroxylation, and irreversible binding of CO can ultimately poison the catalyst. With these binding criteria in mind, the binding energies of H_2 , HCO_2^- , and CO for the series of M_1M_2L complexes were calculated and are plotted in Figure 10. In general, the binding energies for M_1M_2L are stronger when the supporting metal is Ga versus Al. This can be explained by the fact that Ga^{3+} is a stronger Lewis acid toward late transition-metal Lewis bases than Al^{3+} , and as such, it renders the transition metal (Fe, Co, Ni, Pd, Pt) more electron-deficient, which in turn will favor stronger binding of donor ligands. CO, if generated, will effectively poison all the bimetallic catalysts by binding strongly to the metal site, as shown in Figure 10d.

The relative binding free energies of H_2 versus formate change significantly for the different transition metals. The FeML complexes are predicted to bind formate much more strongly than H_2 (FeAlL: $\Delta G_{\rm formate} = -4.4$ kcal/mol vs $\Delta G_{\rm H_2} = 8.7$ kcal/mol; FeGaL: $\Delta G_{\rm formate} = -7.4$ kcal/mol vs $\Delta G_{\rm H_2} = 6.0$ kcal/mol, Figure 10), suggesting that formate would readily block the Fe active site from H_2 binding. For PdML and PtML, both H_2 and HCO_2^- binding energies are endergonic, which would facilitate formate release but make H_2 binding difficult. For CoAlL and NiAlL, the binding of H_2 is slightly endergonic, with formate binding predicted to be less favorable than H_2 binding so as to make the release of formate and the binding of H_2 feasible. For both CoGaL and NiGaL, the H_2 and HCO_2^- binding energies are exergonic and are closely matched, which is optimal for promoting catalytic turnover.

Figure 11 compares the binding energy of H₂ and formate in their van der Waals complexes with Vkd_iPr and [H-(Vkd_iPr)]⁺, respectively. The presence of van der Waals interactions with the base only slightly perturbs the binding favorability for H₂, but it greatly stabilizes the binding of

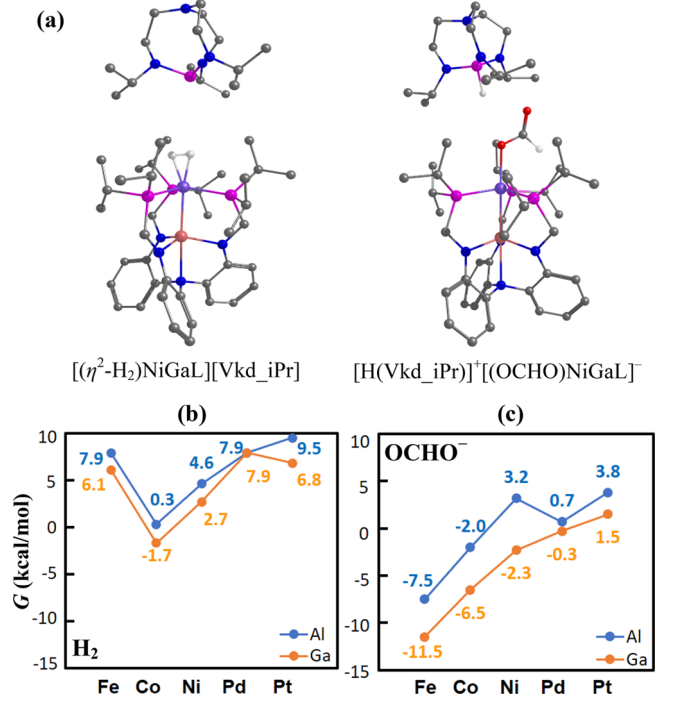


Figure 11. (a) The structure of $[(\eta^2-H_2)NiGaL][Vkd_iPr]$ and $[H(Vkd_iPr)]^+[(OCHO)NiGaL]^-$ (where H atoms bound to carbon atoms are not shown for clarity). The binding energies of H_2 and $OCHO^-$ on M_1M_2L (M_1 = Fe, Co, Ni, Pd, Pt; M_2 = Al, Ga) are plotted in b and c. The color code is the same as in Figure 9.

formate at M_1M_2L , which could result from the electrostatic interaction between the protonated base and formate ions and from the van der Waals interaction between the H atoms of Vkd_iPr and the O atom of formate. Overall, once the electrostatic and van der Waals interactions with base are

considered, the binding energies of formate are much stronger than those of H₂ for all M₁M₂L, indicating that formate would impede the metal active site from binding H2 to a large extent. For NiGaL, H₂ binding is endergonic by 2.7 kcal/mol, while formate binding is exergonic by -2.3 kcal/mol (i.e., formate binding is ~5 kcal/mol more favorable than H₂ binding). On the basis of the criteria of minimizing the amount by which formate binding is more favorable than H₂ binding, CoAlL, CoGaL, NiAlL, and NiGaL are predicted to be the best potential CO₂ hydrogenation catalysts of the bimetallic complexes explored here. Combining this criterion with the previously discussed considerations regarding hydride transfer and H₂ adduct deprotonation, NiGaL and CoGaL are predicted to be the best catalysts among all of the various bimetallics studied in this work because of their hydricity is close to that of formate, the product of hydride transfer to CO₂.

The relative binding energies of H₂ and formate are important because the dissociation of formate was reported to be the rate-determining step for catalysis with NiGaL based on the experimental observation that the anionic formate adduct [(OCHO)NiGaL]⁻ is the catalytic resting state by ³¹P NMR spectroscopy. 47 A similar rate-determining ligand substitution of H₂ for bound formate was predicted for Ru, 58,69 Fe, 45 and Co⁴⁶ catalysts, the latter of which required Li⁺ additives to assist in formate liberation. For NiGaL, the computed thermodynamic binding energetics predict formate binding to be stronger than H₂ binding by ~5 kcal/mol, suggesting a potential impediment to catalytic turnover. Of note, the free energy of activation for formate release (2.3 kcal/ mol) is smaller than the free energy of activation for hydride transfer to CO₂ (12.2 kcal/mol), which is calculated to be the primary rate-determining step after the sufficient buildup of formate lowers the H₂ deprotonation barrier. Considering the significantly larger activation barrier for hydride transfer relative to formate release, the predicted catalyst resting state ought to be the anionic Ni hydride species, [(HCO₂)NiGaL]⁻. We note, however, that solvation energies for small ions like formate can be challenging to calculate accurately, and hence, some uncertainty will exist in this quantitative computational analysis. Of interest, an intriguing experimental observation may help to reconcile this discrepancy between experiment and theory in regard to whether the expected resting state of the catalyst should be the anionic formate adduct or the anionic Ni hydride. Upon the replacement of H_2/CO_2 with $D_2/^{13}CO_2$, both [DNiGaL] and [(D13CO2)NiGaL] were observed during catalysis by in situ 31P NMR spectroscopy, in contrast to only [(HCO₂)NiGaL]⁻ being observed as the catalytic resting state with H₂/CO₂ (Figure S3). While we do not fully understand the underlying basis for these isotopic effects, the detection of both $[DNiGaL]^-$ and $[(D^{13}CO_2)NiGaL]^-$ bridges the apparent discrepancy between experiment and theory by suggesting that hydride transfer and formate dissociation likely have somewhat similar free energies of activation, such that using heavier isotopomers puts the two barriers on par with one another by slowing hydride transfer and resulting in the buildup of both of the aforementioned species during catalysis.

4. CONCLUDING REMARKS

We presented a DFT computational study on the full reaction mechanism for CO_2 hydrogenation catalyzed by a bimetallic NiGaL catalyst, and we also presented supporting experimental work. We found that the most favorable pathway for CO_2 hydrogenation consists of H_2 binding and deprotonation, outer-

sphere hydride transfer to CO_2 , and formate release (Scheme 2). For H_2 deprotonation, the activation barrier depends on the basicity and even more strongly on the steric hindrance of the base. Furthermore, we identified a cocatalytic role of formate in the H_2 deprotonation step, where it acts as a proton shuttle between $(\eta^2\text{-}H_2)\text{NiGaL}$ and Verkade's base and thereby dramatically reduces the activation barrier from 27.8 kcal/mol using Verkade's base alone to 2.7 kcal/mol. With the assistance of formate, the overall rate-determining step is predicted to switch from H_2 deprotonation to hydride transfer to CO_2 . Meanwhile, the stronger binding of formate as compared to H_2 suggests that the formate release is also a step which likely impedes catalysis, and it has been experimentally observed that formate release likely has a free energy of activation that is slightly greater than that of hydride transfer to CO_2 .

To explore the potential of various bimetallic catalyst candidates, we have investigated two series of bimetallic complexes: (1) M_1-M_2 , where M_1 = Fe, Co, Pd, or Pt and $M_2 = Al$ or Ga, and (2) Ni $-M_2$, where $M_2 = Fe$, Co, Al, Ga, or In. For hydride transfer, the free energy of activation for hydride transfer to CO₂ is found to scale linearly with the thermodynamic hydricity of the metal hydride. For the Ni-M series, thermodynamic hydricity can be tuned by 15 kcal/mol simply by varying the supporting Lewis acidic ions. A subset of the bimetallic hydride complexes (where M_1M_2 = FeGa, CoGa, NiGa, and NiIn) has thermodynamic hydricities close to the value of formate, which are considered optimal for catalysis, where $\Delta G^{\circ}_{H^{-}}$ is between 30 and 44 kcal/mol. These linear relationships provide a simple and efficient way to compute the free energies of activation for hydride transfer to CO2. For formate release, several bimetallic complexes (CoAlL, CoGaL, NiAlL, and NiGaL) were identified as potentially promising catalysts based on the relative binding free energies of H2 and formate being neither too weak nor strong, and thereby facilitating catalytic turnover by allowing for the release of formate and rebinding of H2. Thus, while the identified linear relations between the thermodynamics and kinetics of hydride transfer provide a means for rapidly screening the other potential bimetallic catalysts, it is also necessary to analyze the relative free binding energies of H2 and formate to predict the overall catalytic reactivity. Overall, taking into account hydride generation, transfer to CO2, and subsequent formate release, NiGaL and CoGaL are predicted to be the best catalysts among all of the various bimetallics studied.

In addition to identifying CoGaL as a promising catalyst for future study, our detailed mechanistic study has identified strategies to further improve the efficiency of the NiGaL catalyst in CO₂ hydrogenation. Specifically, reducing the steric bulk of the phosphine substituents of NiGaL and of the base may allow for more facile deprotonation by weaker and less expensive bases. Additional considerations include optimizing the hydricity of bimetallic complexes so as to maintain potent reactivity while still allowing facile metal hydride generation from H2, as well as maximizing the favorability of H2 binding relative to formate binding. Among the complexes surveyed, the only other bimetallic catalyst besides NiGaL that strongly meets these identified criteria is CoGaL, which we plan to investigate in future studies. The present computational results provide guidance to future experimental work and build a strong foundation for understanding trends as we seek to optimize catalysis by expanding our investigation to a larger series of bimetallic catalysts.

ASSOCIATED CONTENT

S Supporting Information

The Supporting Information is available free of charge on the ACS Publications website at DOI: 10.1021/acscatal.8b00803.

Figures S1-S4, Tables S1-S5, and energies and coordinates of structures (PDF)

AUTHOR INFORMATION

Corresponding Authors

*E-mail: jye@umn.edu. *E-mail: clu@umn.edu.

ORCID ®

Jingyun Ye: 0000-0003-4373-9625 Jing Xie: 0000-0001-9676-5734

Donald G. Truhlar: 0000-0002-7742-7294 Christopher J. Cramer: 0000-0001-5048-1859

Connie C. Lu: 0000-0002-5162-9250 Laura Gagliardi: 0000-0001-5227-1396

Notes

The authors declare no competing financial interest.

ACKNOWLEDGMENTS

This work was supported as part of the Inorganometallic Catalyst Design Center, an EFRC funded by the DOE, Office of Basic Energy Sciences (DE-SC0012702). The computations were performed at the Minnesota Supercomputing Institute and National Energy Research Scientific Computing Center under project 36159. R.C.C., M.V.V., and C.C.L. are supported by the National Science Foundation (CHE-1665010).

REFERENCES

- (1) Aresta, M.; Dibenedetto, A.; Angelini, A. Catalysis for the Valorization of Exhaust Carbon: From CO₂ to Chemicals, Materials, and Fuels. Technological Use of CO₂. *Chem. Rev.* **2014**, *114*, 1709–1742.
- (2) Boden, T. A.; Andres, R. J.; Marland, G. Global, Regional, and National Fossil-Fuel CO_2 Emissions. In *Trends: A Compendium of Data on Global Change*; Carbon Dioxide Information Analysis Center, Oak Ridge National Laboratory, U.S. Department of Energy, Oak Ridge, TN. 2017.
- (3) Le Quéré, C.; Moriarty, R.; Andrew, R. M.; Canadell, J. G.; Sitch, S.; Korsbakken, J. I.; Friedlingstein, P.; Peters, G. P.; Andres, R. J.; Boden, T. A.; Houghton, R. A.; House, J. I.; Keeling, R. F.; Tans, P.; Arneth, A.; Bakker, D. C. E.; Barbero, L.; Bopp, L.; Chang, J.; Chevallier, F.; Chini, L. P.; Ciais, P.; Fader, M.; Feely, R. A.; Gkritzalis, T.; Harris, I.; Hauck, J.; Ilyina, T.; Jain, A. K.; Kato, E.; Kitidis, V.; Klein Goldewijk, K.; Koven, C.; Landschützer, P.; Lauvset, S. K.; Lefèvre, N.; Lenton; Murata, A.; Lima, I. D.; Metzl, N.; Millero, F.; Munro, D. R. A.; Nabel, J. E. M. S.; Nakaoka, S.; Nojiri, Y.; O'Brien, K.; Olsen, A.; Ono, T.; Pérez, F. F.; Pfeil, B.; Pierrot, D.; Poulter, B.; Rehder, G.; Rödenbeck, C.; Saito, S.; Schuster, U.; Schwinger, J.; Séférian, R.; Steinhoff, T.; Stocker, B. D.; Sutton, A. J.; Takahashi, T.; Tilbrook, B.; van der Laan-Luijkx, I. T.; van der Werf, G. R.; van Heuven, S.; Vandemark, D.; Viovy, N.; Wiltshire, A.; Zaehle, S.; Zeng, N. Global Carbon Budget 2015. Earth Syst. Sci. Data 2015, 7 (2), 349-396.
- (4) Dlugokencky, E.; Tans, P. NOAA/ESRL (www.esrl.noaa.gov/gmd/ccgg/trends/).
- (5) Jacobson, M. Z. Climate Response of Fossil Fuel and Biofuel Soot, Accounting for Soot's Feedback to Snow and Sea Ice Albedo and Emissivity. *J. Geophys. Res. Atmos.* **2004**, *109*, D21201.
- (6) Jacobson, M. Z. Control of Fossil-Fuel Particulate Black Carbon and Organic Matter, Possibly the Most Effective Method of Slowing Global Warming. *J. Geophys. Res.* **2002**, *107*, 4410.

- (7) Kondratenko, E. V.; Mul, G.; Baltrusaitis, J.; Larrazábal, G. O.; Pérez-Ramírez, J. Status and Perspectives of CO₂ Conversion into Fuels and Chemicals by Catalytic, Photocatalytic and Electrocatalytic Processes. *Energy Environ. Sci.* **2013**, *6*, 3112.
- (8) Appel, A. M.; Bercaw, J. E.; Bocarsly, A. B.; Dobbek, H.; DuBois, D. L.; Dupuis, M.; Ferry, J. G.; Fujita, E.; Hille, R.; Kenis, P. J. A.; Kerfeld, C. A.; Morris, R. H.; Peden, C. H. F.; Portis, A. R.; Ragsdale, S. W.; Rauchfuss, T. B.; Reek, J. N. H.; Seefeldt, L. C.; Thauer, R. K.; Waldrop, G. L. Frontiers, Opportunities, and Challenges in Biochemical and Chemical Catalysis of CO₂ Fixation. *Chem. Rev.* **2013**, *113*, 6621–6658.
- (9) Benson, E. E.; Kubiak, C. P.; Sathrum, A. J.; Smieja, J. M. Electrocatalytic and Homogeneous Approaches to Conversion of CO₂ to Liquid Fuels. *Chem. Soc. Rev.* **2009**, *38*, 89–99.
- (10) Goeppert, A.; Czaun, M.; Jones, J.-P.; Surya Prakash, G. K.; Olah, G. A. Recycling of Carbon Dioxide to Methanol and Derived Products Closing the Loop. *Chem. Soc. Rev.* **2014**, *43*, 7995–8048.
- (11) Olah, G. A.; Prakash, G. K. S.; Goeppert, A. Anthropogenic Chemical Carbon Cycle for a Sustainable Future. *J. Am. Chem. Soc.* **2011**, *133*, 12881–12898.
- (12) Klankermayer, J.; Wesselbaum, S.; Beydoun, K.; Leitner, W. Selective Catalytic Synthesis Using the Combination of Carbon Dioxide and Hydrogen: Catalytic Chess at the Interface of Energy and Chemistry. *Angew. Chem., Int. Ed.* **2016**, *55*, 7296–7343.
- (13) Wang, W.-H.; Himeda, Y.; Muckerman, J. T.; Manbeck, G. F.; Fujita, E. CO₂ Hydrogenation to Formate and Methanol as an Alternative to Photo- and Electrochemical CO₂ Reduction. *Chem. Rev.* **2015**, *115*, 12936–12973.
- (14) Álvarez, A.; Bansode, A.; Urakawa, A.; Bavykina, A. V.; Wezendonk, T. A.; Makkee, M.; Gascon, J.; Kapteijn, F. Challenges in the Greener Production of Formates/Formic Acid, Methanol, and DME by Heterogeneously Catalyzed CO₂ Hydrogenation Processes. *Chem. Rev.* **2017**, *117*, 9804–9838.
- (15) Boddien, A.; Mellmann, D.; Gärtner, F.; Jackstell, R.; Junge, H.; Dyson, P. J.; Laurenczy, G.; Ludwig, R.; Beller, M. Efficient Dehydrogenation of Formic Acid Using an Iron Catalyst. *Science* **2011**, 333, 1733–1736.
- (16) Rice, C.; Ha, S.; Masel, R. I.; Waszczuk, P.; Wieckowski, A.; Barnard, T. Direct Formic Acid Fuel Cells. *J. Power Sources* **2002**, *111*, 83–89.
- (17) Li, Z.; Xu, Q. Metal-Nanoparticle-Catalyzed Hydrogen Generation from Formic Acid. *Acc. Chem. Res.* **2017**, *50*, 1449–1458. (18) Du, D.; Lan, R.; Humphreys, J.; Tao, S. Progress in Inorganic Cathode Catalysts for Electrochemical Conversion of Carbon Dioxide into Formate or Formic Acid. *J. Appl. Electrochem.* **2017**, *47*, 661–678.
- (19) Bernskoetter, W. H.; Hazari, N. Reversible Hydrogenation of Carbon Dioxide to Formic Acid and Methanol: Lewis Acid Enhancement of Base Metal Catalysts. *Acc. Chem. Res.* **2017**, *50*, 1049–1058.
- (20) Mellmann, D.; Sponholz, P.; Junge, H.; Beller, M. Formic Acid as a Hydrogen Storage Material Development of Homogeneous Catalysts for Selective Hydrogen Release. *Chem. Soc. Rev.* **2016**, *45*, 3954—3988.
- (21) Jessop, P. G.; Joó, F.; Tai, C.-C. Recent Advances in the Homogeneous Hydrogenation of Carbon Dioxide. *Coord. Chem. Rev.* **2004**, 248, 2425–2442.
- (22) Federsel, C.; Jackstell, R.; Beller, M. State-of-the-Art Catalysts for Hydrogenation of Carbon Dioxide. *Angew. Chem., Int. Ed.* **2010**, *49*, 6254–6257.
- (23) Munshi, P.; Main, A. D.; Linehan, J. C.; Tai, C.-C.; Jessop, P. G. Hydrogenation of Carbon Dioxide Catalyzed by Ruthenium Trimethylphosphine Complexes: The Accelerating Effect of Certain Alcohols and Amines. *J. Am. Chem. Soc.* **2002**, *124*, 7963–7971.
- (24) Elek, J.; Nádasdi, L.; Papp, G.; Laurenczy, G.; Joó, F. Homogeneous Hydrogenation of Carbon Dioxide and Bicarbonate in Aqueous Solution Catalyzed by Water-Soluble ruthenium(II) Phosphine Complexes. *Appl. Catal., A* **2003**, *255*, 59–67.

(25) Schaub, T.; Paciello, R. A. A Process for the Synthesis of Formic Acid by CO₂ Hydrogenation: Thermodynamic Aspects and the Role of CO. *Angew. Chem., Int. Ed.* **2011**, *50*, 7278–7282.

- (26) Sanz, S.; Azua, A.; Peris, E. (η^6 -arene)Ru(bis-NHC)" Complexes for the Reduction of CO₂ to Formate with Hydrogen and by Transfer Hydrogenation with iPrOH. *Dalt. Trans.* **2010**, *39*, 6339–6343.
- (27) Filonenko, G. A.; Smykowski, D.; Szyja, B. M.; Li, G.; Szczygieł, J.; Hensen, E. J. M.; Pidko, E. A. Catalytic Hydrogenation of CO_2 to Formates by a Lutidine-Derived Ru–CNC Pincer Complex: Theoretical Insight into the Unrealized Potential. *ACS Catal.* **2015**, 5, 1145–1154.
- (28) Planas, N.; Ono, T.; Vaquer, L.; Miró, P.; Benet-Buchholz, J.; Gagliardi, L.; Cramer, C. J.; Llobet, A. Carbon Dioxide Reduction by Mononuclear Ruthenium Polypyridyl Complexes. *Phys. Chem. Chem. Phys.* **2011**, *13*, 19480–19484.
- (29) Ono, T.; Qu, S.; Gimbert-Suriñach, C.; Johnson, M. A.; Marell, D. J.; Benet-Buchholz, J.; Cramer, C. J.; Llobet, A. Hydrogenative Carbon Dioxide Reduction Catalyzed by Mononuclear Ruthenium Polypyridyl Complexes: Discerning between Electronic and Steric Effects. ACS Catal. 2017, 7, 5932–5940.
- (30) Graf, E.; Leitner, W. Direct Formation of Formic Acid from Carbon Dioxide and Dihydrogen Using the [{Rh(cod)Cl}₂]-Ph₂P-(CH₂)₄PPh₂ Catalyst System. *J. Chem. Soc., Chem. Commun.* **1992**, 387, 623–624.
- (31) Ezhova, N. N.; Kolesnichenko, N. V.; Bulygin, A. V.; Slivinskii, E. V.; Han, S. Hydrogenation of CO₂ to Formic Acid in the Presence of the Wilkinson Complex. *Russ. Chem. Bull.* **2002**, *51*, 2165–2169.
- (32) Musashi, Y.; Sakaki, S. Theoretical Study of Rhodium(III)-Catalyzed Hydrogenation of Carbon Dioxide into Formic Acid. Significant Differences in Reactivity among Rhodium(III), Rhodium-(I), and Ruthenium(II) Complexes. J. Am. Chem. Soc. 2002, 124, 7588–7603.
- (33) Hutschka, F.; Dedieu, A.; Eichberger, M.; Fornika, R.; Leitner, W. Mechanistic Aspects of the Rhodium-Catalyzed Hydrogenation of CO₂ to Formic Acid-A Theoretical and Kinetic Study. *J. Am. Chem. Soc.* 1997, 119, 4432–4443.
- (34) Tanaka, R.; Yamashita, M.; Nozaki, K. Catalytic Hydrogenation of Carbon Dioxide Using Ir(III)—Pincer Complexes. *J. Am. Chem. Soc.* **2009**, *131*, 14168—14169.
- (35) Himeda, Y. Conversion of CO₂ into Formate by Homogeneously Catalyzed Hydrogenation in Water: Tuning Catalytic Activity and Water Solubility through the Acid–Base Equilibrium of the Ligand. *Eur. J. Inorg. Chem.* **2007**, 2007, 3927–3941.
- (36) Schmeier, T. J.; Dobereiner, G. E.; Crabtree, R. H.; Hazari, N. Secondary Coordination Sphere Interactions Facilitate the Insertion Step in an Iridium(III) CO₂ Reduction Catalyst. *J. Am. Chem. Soc.* **2011**, 133, 9274–9277.
- (37) Hull, J. F.; Himeda, Y.; Wang, W.-H.; Hashiguchi, B.; Periana, R.; Szalda, D. J.; Fujita, E.; Muckerman, J. T. Reversible Hydrogen Storage Using CO₂ and a Proton-Switchable Iridium Catalyst in Aqueous Media under Mild Temperatures and Pressures. *Nat. Chem.* **2012**, *4*, 383–388.
- (38) Filonenko, G. A.; Hensen, E. J. M.; Pidko, E. A. Mechanism of CO₂ Hydrogenation to Formates by Homogeneous Ru-PNP Pincer Catalyst: From a Theoretical Description to Performance Optimization. *Catal. Sci. Technol.* **2014**, *4*, 3474–3485.
- (39) Schneidewind, J.; Adam, R.; Baumann, W.; Jackstell, R.; Beller, M. Low-Temperature Hydrogenation of Carbon Dioxide to Methanol with a Homogeneous Cobalt Catalyst. *Angew. Chem., Int. Ed.* **2017**, *56*, 1890–1893.
- (40) Langer, R.; Diskin-Posner, Y.; Leitus, G.; Shimon, L. J. W.; Ben-David, Y.; Milstein, D. Low-Pressure Hydrogenation of Carbon Dioxide Catalyzed by an Iron Pincer Complex Exhibiting Noble Metal Activity. *Angew. Chem., Int. Ed.* **2011**, *50*, 9948–9952.
- (41) Ziebart, C.; Federsel, C.; Anbarasan, P.; Jackstell, R.; Baumann, W.; Spannenberg, A.; Beller, M. Well-Defined Iron Catalyst for Improved Hydrogenation of Carbon Dioxide and Bicarbonate. *J. Am. Chem. Soc.* **2012**, *134*, 20701–20704.

- (42) Federsel, C.; Ziebart, C.; Jackstell, R.; Baumann, W.; Beller, M. Catalytic Hydrogenation of Carbon Dioxide and Bicarbonates with a Well-Defined Cobalt Dihydrogen Complex. *Chem. Eur. J.* **2012**, *18*, 72–75.
- (43) Zell, T.; Milstein, D. Hydrogenation and Dehydrogenation Iron Pincer Catalysts Capable of Metal—Ligand Cooperation by Aromatization/Dearomatization. *Acc. Chem. Res.* **2015**, *48*, 1979—1994.
- (44) Jeletic, M. S.; Mock, M. T.; Appel, A. M.; Linehan, J. C. A Cobalt-Based Catalyst for the Hydrogenation of CO₂ under Ambient Conditions. *J. Am. Chem. Soc.* **2013**, *135*, 11533–11536.
- (45) Zhang, Y.; MacIntosh, A. D.; Wong, J. L.; Bielinski, E. A.; Williard, P. G.; Mercado, B. Q.; Hazari, N.; Bernskoetter, W. H. Iron Catalyzed CO₂ Hydrogenation to Formate Enhanced by Lewis Acid Co-Catalysts. *Chem. Sci.* **2015**, *6*, 4291–4299.
- (46) Spentzos, A. Z.; Barnes, C. L.; Bernskoetter, W. H. Effective Pincer Cobalt Precatalysts for Lewis Acid Assisted CO₂ Hydrogenation. *Inorg. Chem.* **2016**, *55*, 8225–8233.
- (47) Cammarota, R. C.; Vollmer, M. V.; Xie, J.; Ye, J.; Linehan, J. C.; Burgess, S. A.; Appel, A. M.; Gagliardi, L.; Lu, C. C. A Bimetallic Nickel-Gallium Complex Catalyses CO₂ Hydrogenation via the Intermediacy of an Anionic d10 Nickel-Hydride. *J. Am. Chem. Soc.* **2017**, 139, 14244–14250.
- (48) Inoue, Y.; Izumida, H.; Sasaki, Y.; Hashimoto, H. Catalytic Fixation of Carbon Dioxide to Formic Acid by Transition-Metal Complexes under Mild Conditions. *Chem. Lett.* **1976**, *5*, 863–864.
- (49) Burgess, S. A.; Kendall, A. J.; Tyler, D. R.; Linehan, J. C.; Appel, A. M. Hydrogenation of CO₂ in Water Using a Bis(diphosphine) Ni–H Complex. *ACS Catal.* **2017**, *7*, 3089–3096.
- (50) Enthaler, S.; Brück, A.; Kammer, A.; Junge, H.; Irran, E.; Gülak, S. Exploring the Reactivity of Nickel Pincer Complexes in the Decomposition of Formic Acid to CO_2/H_2 and the Hydrogenation of NaHCO $_3$ to HCOONa. *ChemCatChem* **2015**, *7*, 65–69.
- (51) Frisch, M. J.; Trucks, G. W.; Schlegel, H. B.; Scuseria, G. E.; Robb, M. A.; Cheeseman, J. R.; Scalmani, G.; Barone, V.; Mennucci, B.; Petersson, G. A.; Nakatsuji, H.; Caricato, M.; Li, X.; Hratchian, H. P.; Izmaylov, A. F.; Bloino, J.; Zheng, G.; Sonnenberg, J. L.; Hada, M.; Ehara, M.; Toyota, K.; Fukuda, R.; Hasegawa, J.; Ishida, M.; Nakajima, T.; Honda, Y.; Kitao, O.; Nakai, H.; Vreven, T.; Montgomery, J. A., Jr.; Peralta, J. E.; Ogliaro, F.; Bearpark, M.; Heyd, J. J.; Brothers, E.; Kudin, K. N.; Staroverov, V. N.; Kobayashi, R.; Normand, J.; Raghavachari, K.; Rendell, A.; Burant, J. C.; Iyengar, S. S.; Tomasi, J.; Cossi, M.; Rega, N.; Millam, J. M.; Klene, M.; Knox, J. E.; Cross, J. B.; Bakken, V.; Adamo, C.; Jaramillo, J.; Gomperts, R.; Stratmann, R. E.; Yazyev, O.; Austin, A. J.; Cammi, R.; Pomelli, C.; Ochterski, J. W.; Martin, R. L.; Morokuma, K.; Zakrzewski, V. G.; Voth, G. A.; Salvador, P.; Dannenberg, J. J.; Dapprich, S.; Daniels, A. D.; Farkas, Ö.; Foresman, J. B.; Ortiz, J. V.; Cioslowski, J.; Fox, D. J. Gaussian 09, revision E.01; Gaussian, Inc.: Wallingford, CT, 2009.
- (52) Zhao, Y.; Truhlar, D. G. A New Local Density Functional for Main-Group Thermochemistry, Transition Metal Bonding, Thermochemical Kinetics, and Noncovalent Interactions. *J. Chem. Phys.* **2006**, 125, 194101.
- (53) Weigend, F.; Hättig, C.; Patzelt, H.; Ahlrichs, R.; Spencer, S.; Willets, A. Accurate Coulomb-Fitting Basis Sets for H to Rn. *Phys. Chem. Chem. Phys.* **2006**, *8*, 1057–1065.
- (54) Weigend, F.; Ahlrichs, R. Balanced Basis Sets of Split Valence, Triple Zeta Valence and Quadruple Zeta Valence Quality for H to Rn: Design and Assessment of Accuracy. *Phys. Chem. Chem. Phys.* **2005**, *7*, 3297–3305.
- (55) Andrae, D.; Häußermann, U.; Dolg, M.; Stoll, H.; Preuß, H. Energy-Adjustedab Initio Pseudopotentials for the Second and Third Row Transition Elements. *Theor. Chim. Acta* **1990**, *77*, 123–141.
- (56) Marenich, A. V.; Cramer, C. J.; Truhlar, D. G. Universal Solvation Model Based on Solute Electron Density and on a Continuum Model of the Solvent Defined by the Bulk Dielectric Constant and Atomic Surface Tensions. *J. Phys. Chem. B* **2009**, *113*, 6378–6396.
- (57) Kumar, N.; Camaioni, D. M.; Dupuis, M.; Raugei, S.; Appel, A. M. Mechanistic Insights into Hydride Transfer for Catalytic

Hydrogenation of CO₂ with Cobalt Complexes. *Dalt. Trans.* **2014**, 43, 11803–11806.

- (58) Urakawa, A.; Jutz, F.; Laurenczy, G.; Baiker, A. Carbon Dioxide Hydrogenation Catalyzed by a Ruthenium Dihydride: A DFT and High-Pressure Spectroscopic Investigation. *Chem. Eur. J.* **2007**, *13*, 3886–3899.
- (59) Ni, S.-F.; Dang, L. Insight into the Electronic Effect of Phosphine Ligand on Rh Catalyzed CO₂ Hydrogenation by Investigating the Reaction Mechanism. *Phys. Chem. Chem. Phys.* **2016**, *18*, 4860–4870.
- (60) Batsanov, S. S. Van Der Waals Radii of Elements. *Inorg. Mater.* **2001**, *37*, 871–885.
- (61) Cammarota, R. C.; Lu, C. C. Tuning Nickel with Lewis Acidic Group 13 Metalloligands for Catalytic Olefin Hydrogenation. *J. Am. Chem. Soc.* **2015**, *137*, 12486–12489.
- (62) Zall, C. M.; Linehan, J. C.; Appel, A. M. A Molecular Copper Catalyst for Hydrogenation of CO_2 to Formate. *ACS Catal.* **2015**, *5*, 5301–5305.
- (63) Zall, C. M.; Linehan, J. C.; Appel, A. M. Triphosphine-Ligated Copper Hydrides for CO₂ Hydrogenation: Structure, Reactivity, and Thermodynamic Studies. *J. Am. Chem. Soc.* **2016**, 138, 9968–9977.
- (64) Kisanga, P. B.; Verkade, J. G.; Schwesinger, R. pKa Measurements of P(RNCH₂CH₃)₃N. J. Org. Chem. **2000**, 65, 5431–5432.
- (65) Kaljurand, I.; Kütt, A.; Sooväli, L.; Rodima, T.; Mäemets, V.; Leito, I.; Koppel, I. A. Extension of the Self-Consistent Spectrophotometric Basicity Scale in Acetonitrile to a Full Span of 28 pKa Units: Unification of Different Basicity Scales. *J. Org. Chem.* **2005**, *70*, 1019–1028.
- (66) Ding, F.; Smith, J. M.; Wang, H. First-Principles Calculation of PK_a Values for Organic Acids in Nonaqueous Solution. *J. Org. Chem.* **2009**, 74, 2679–2691.
- (67) Lilio, A. M.; Reineke, M. H.; Moore, C. E.; Rheingold, A. L.; Takase, M. K.; Kubiak, C. P. Incorporation of Pendant Bases into Rh(diphosphine) ₂ Complexes: Synthesis, Thermodynamic Studies, And Catalytic CO₂ Hydrogenation Activity of [Rh(P₂N₂)₂]⁺ Complexes. *J. Am. Chem. Soc.* **2015**, *137*, 8251–8260.
- (68) Elgrishi, N.; Kurtz, D. A.; Dempsey, J. L. Reaction Parameters Influencing Cobalt Hydride Formation Kinetics: Implications for Benchmarking H₂ -Evolution Catalysts. *J. Am. Chem. Soc.* **2017**, *139*, 239–244
- (69) Urakawa, A.; Iannuzzi, M.; Hutter, J.; Baiker, A. Towards a Rational Design of Ruthenium CO₂ Hydrogenation Catalysts by Ab Initio Metadynamics. *Chem. Eur. J.* **2007**, *13*, 6828–6840.
- (70) Wiedner, E. S.; Chambers, M. B.; Pitman, C. L.; Bullock, R. M.; Miller, A. J. M.; Appel, A. M. Thermodynamic Hydricity of Transition Metal Hydrides. *Chem. Rev.* **2016**, *116*, 8655–8692.
- (71) Jessop, P. G.; Ikariya, T.; Noyori, R. Homogeneous Hydrogenation of Carbon Dioxide. *Chem. Rev.* **1995**, *95*, 259–272.
- (72) Rohmann, K.; Kothe, J.; Haenel, M. W.; Englert, U.; Hölscher, M.; Leitner, W. Hydrogenation of CO₂ to Formic Acid with a Highly Active Ruthenium Acriphos Complex in DMSO and DMSO/Water. *Angew. Chem., Int. Ed.* **2016**, *55*, 8966–8969.
- (73) Muckerman, J. T.; Achord, P.; Creutz, C.; Polyansky, D. E.; Fujita, E. Calculation of Thermodynamic Hydricities and the Design of Hydride Donors for CO₂ Reduction. *Proc. Natl. Acad. Sci. U. S. A.* **2012**, *109*, 15657–15662.
- (74) Qi, X.-J.; Fu, Y.; Liu, L.; Guo, Q.-X. Ab Initio Calculations of Thermodynamic Hydricities of Transition-Metal Hydrides in Acetonitrile. *Organometallics* **2007**, *26*, 4197–4203.
- (75) Rudd, P. A.; Liu, S.; Gagliardi, L.; Young, V. G.; Lu, C. C. Metal—Alane Adducts with Zero-Valent Nickel, Cobalt, and Iron. J. Am. Chem. Soc. 2011, 133, 20724—20727.
- (76) Curtis, C. J.; Miedaner, A.; Ellis, W. A.; DuBois, D. L. Measurement of the Hydride Donor Abilities of [HM(diphosphine)₂]⁺ Complexes (M = Ni, Pt) by Heterolytic Activation of Hydrogen. *J. Am. Chem. Soc.* **2002**, *124*, 1918–1925.
- (77) Ciancanelli, R.; Noll, B. C.; DuBois, D. L.; DuBois, M. R. Comprehensive Thermodynamic Characterization of the Metal—

- Hydrogen Bond in a Series of Cobalt-Hydride Complexes. J. Am. Chem. Soc. 2002, 124, 2984–2992.
- (78) Mondal, B.; Neese, F.; Ye, S. Toward Rational Design of 3d Transition Metal Catalysts for CO ₂ Hydrogenation Based on Insights into Hydricity-Controlled Rate-Determining Steps. *Inorg. Chem.* **2016**, *55*, 5438–5444.
- (79) Jeletic, M. S.; Helm, M. L.; Hulley, E. B.; Mock, M. T.; Appel, A. M.; Linehan, J. C. A Cobalt Hydride Catalyst for the Hydrogenation of CO₂: Pathways for Catalysis and Deactivation. *ACS Catal.* **2014**, *4*, 3755–3762.